Distributed Collaborative Beamforming Design in Scattered-Environments

Slim Zaidi, *Student Member*, *IEEE*, and Sofiène Affes, *Senior Member*, *IEEE*

***Abstract*—In this paper, we consider a collaborative beamforming (CB) technique to achieve a dual-hop communication from a source surrounded by M_I interferences to a receiver, through a wireless network comprised of K independent terminals. The CB weights are designed so as to minimize the interferences plus noises' powers while maintaining the received power from the source to a constant level. We show, however, that they are intractable in closed-form due to the complexity of the polychromatic channels arising from the presence of scattering in real-world environments. By recurring to a two-ray channel approximation proved valid at relatively low angular spread (AS) values, we are able to derive the new optimum weights and prove that they could be locally computed at each terminal, thereby complying with the distributed feature of the network of interest. The so-obtained bichromatic distributed collaborative beamforming (B-DCB) is then analyzed and compared in performance to the monochromatic CB (MCB), whose design does not account for scattering, and the optimal CSI-based CB (OCB). It is shown that the proposed B-DCB outperforms its counterparts in real-world environments.**

***Index Terms*—Distributed collaborative beamforming, scattering, angular distribution/spread, interference, wireless sensor networks (WSN).**

I. Introduction

The widely used CB solution that is able to handle both scattering and interference, both present in almost all real-world scenarios, is the optimal CSI-based CB (OCB) [1]-[3]. When the latter is implemented in the network, it has been shown that each collaborating terminal's weight then depends not only on that terminal's CSI, but also on the other terminals' CSI [1]-[3] [4] [5]. Since terminals are very often autonomous and located at different physical locations, they have limited knowledge about each other's CSI. To compute their respective interdependent weights, they have to exchange their local information resulting inevitably in an undesired overhead. The latter increases with the terminals' number K, the interferences' number M_I as well as the channel Doppler frequencies [4] [5]. If one of these parameters is large, this overhead becomes prohibitive and may cause substantial performance degradation and severe terminals' power depletion. This critical impediment motivates further investigation of strategies able to reduce the overhead incurred by OCB.

As such, the optimized CSI or weights' quantization schemes such as the Grassmannian scheme in [6] appear to be efficient strategies to achieve this goal. Nevertheless, the latter usually require a huge codebook that increases the overall cost of the network if integrated at each terminal. Furthermore, the quantization itself introduces errors in weights, thereby causing a CB's performance degradation. More importantly, such schemes do not significantly reduce overhead since the latter still keeps increasing with K, M_I, and channel Doppler frequencies. Another strategy to circumvent this problem consists in ignoring scattering and assuming instead monochromatic (i.e, single-ray) channels. This assumption allows terminals to avoid CSI estimation since the latter will then only depend on each terminal's location and the source and interference DoAs [7]. Several monochromatic CBs (MCB)s have been proposed [7]-[9], but unfortunately shown [10]-[12] to perform poorly over polychromatic (i.e., multi-ray) channels due to mismatch. At very small values of the angular spread (AS), the latter results into slight deterioration that becomes, however, quickly unsatisfactory at moderate to large AS. In other words, any overhead gain of MCB against OCB can be achieved only at the expense of some performance loss. Furthermore, this gain is far from being sufficient since MCB's overhead remains linearly dependent on K and M_I. This work aims precisely to develop a new CB solution that approaches the OCB's high performance level at an overhead-cost much lower than the MCB's overhead.

In this paper, we consider an OCB design to achieve a dual-hop communication from a source surrounded by M_I interferences to a receiver, through a wireless network comprised of K independent terminals. The CB weights are designed so as to minimize the interferences plus noises' powers while maintaining the received power from the source to a constant level. We show, however, that they are intractable in closed-form due to the complexity of the polychromatic channels arising from the presence of scattering in real-world environments. By recurring to a two-ray channel approximation proved valid at relatively low angular spread (AS) values, we are able to derive the new optimum weights and prove that they could be locally computed at each terminal, thereby complying with the distributed feature of the network of interest. It is shown that the so-obtained bichromatic distributed collaborative beamforming (B-DCB) outperforms in real-world environments both OCB and MCB.

II. System model

As illustrated in Fig. 1, the system of interest consists of a wireless network or subnetwork comprised of K terminals equipped each with a single isotropic antenna and uniformly and independently distributed on $D(O,R)$, the disc with center at O and radius R, a receiver Rx, and M far-field sources including a desired source $S_{\rm d}$ and M_I interfering sources. All sources are located in the same plane containing $D(O,R)$ [7] [8]. We assume that there is no direct link from the latters to the receiver due to high pathloss attenuation. Moreover, let (r_k,ψ_k) denote the polar coordinates of the k-th terminal and (A_m,ϕ_m) those of the m-th source. Without loss of generality, (A_1,ϕ_1) is assumed to be the location of $S_{\rm d}$ with $\phi_1=0$. Since the sources are in the far-field, we hence assume that $A_m \gg R$ for $m=1,\ldots,M$ where $M=M_I+1$. The following assumptions are further adopted throughout this paper:

Work supported by the CRD, DG, and CREATE PERSWADE Programs of NSERC and a Discovery Accelerator Supplement Award from NSERC.

978-1-4673-6555-0/15/$31.00 ©2015 IEEE

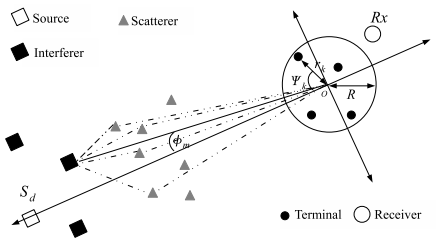

Fig. 1. System model.

A1) The m-th source is scattered by a given number of scatterers located in the same plane containing $D(O,R)$. The latter generate from the transmit signal L_m rays or "spatial chromatics" (with reference to their angular distribution) that form a polychromatic propagation channel [10]-[11]. The l-th ray or chromatic is characterized by its angle deviation $\theta_{l,m}$ from the m-th source direction ϕ_m and its complex amplitude $\alpha_{l,m}$. The $\theta_{l,m},\ l=1,\ldots,L$ are i.i.d. zero-mean random variables with a symmetric probability density function (pdf) $p_m(\theta)$ and variance σ_m^2. Note that the standard deviation σ_m is commonly known as the angular spread (AS) while $p_m(\theta)$ is called the scattering or angular distribution [10]-[11]. The $\alpha_{l,m}\ l=1,\ldots,L$ are i.i.d zero-mean random variables with $\mathrm{E}\left\{|\alpha_{l,m}|^2\right\}=1/L_m$. All $\theta_{l,m}$ and $\alpha_{l,m}$ for $m=1,\ldots,M$ and $l=1,\ldots,L_m$ are assumed to be mutually independent.

A2) The forward channel gain $[\mathbf{f}]_k$ from the k-th terminal to the receiver is a zero-mean unit-variance circular Gaussian random variable [11].

A3) The m-th source's signal s_m is narrow-band zero-mean random variable with power p_m while noises at terminals and the receiver are zero-mean Gaussian random variables with variances $\sigma_{n_t}^2$ and $\sigma_{n_r}^2$, respectively. All signals, noises, and the terminals' forward channel gains are mutually independent.

A4) The k-th terminal is only aware of its own coordinates (r_k,ψ_k), its forward channel $[\mathbf{f}]_k$, K, the wavelength λ while being oblivious to the locations and the forward channels of *all* other terminals in the network.

Recurring to A1 and the fact that $A_m \gg R$ for $m=1,\ldots,M$, the backward channel gain from the m-th source to the k-th terminal can be represented as $[\mathbf{g}_m]_k=\sum_{l=1}^{L_m}\alpha_{l,m}e^{-j\frac{2\pi}{\lambda}r_k\cos(\phi_m+\theta_{l,m}-\psi_k)}$. Obviously, when the scattering effect is neglected (i.e., $\sigma_m \longrightarrow 0$) to assume a monochromatic plane-wave propagation channel, we have $\theta_{l,m}=0$ and, hence, $[\mathbf{g}_m]_k$ could be reduced to $\left[\mathbf{g}_m^{(1)}\right]_k=e^{-j(2\pi/\lambda)r_k\cos(\phi_m-\psi_k)}$, the well-known steering vector element in the array-processing literature [7]-[11].

The communication link between the desired source S_{d} and the receiver is established using the following dual-hop scheme. In the first time slot, all sources send their signals to the wireless network while, in the second time slot, the k-th terminal multiplies its received signal with the complex conjugate of its beamforming weight w_k and forwards the resulting signal to the receiver Rx. It can be readily shown that the desired power received from S_{d} is $P_{\mathbf{w},d}=p_1\mathbf{w}^H\mathrm{E}\left\{\mathbf{h}_1\mathbf{h}_1^H\right\}\mathbf{w}$ while the undesired power from both the interference and noise is $P_{\mathbf{w},u}=\mathbf{w}^H\mathrm{E}\left\{\mathbf{H}_{\bar{1}}\mathbf{P}_{\bar{1}}\mathbf{H}_{\bar{1}}^H\right\}\mathbf{w}+\sigma_{n_t}^2\mathbf{w}^H\mathbf{\Sigma}\mathbf{w}+\sigma_{n_r}^2$ where $\mathbf{H}_{\bar{1}}\triangleq[\mathbf{f}\odot\mathbf{g}_2\ldots\mathbf{f}\odot\mathbf{g}_M]$ with $\mathbf{f}\triangleq[[\mathbf{f}]_1\ldots[\mathbf{f}]_K]^T$, $\mathbf{P}_{\bar{1}}\triangleq\mathrm{diag}\{p_2\ldots p_M\}$, $\mathbf{\Sigma}\triangleq\mathrm{diag}\{|[\mathbf{f}]_1|^2\ldots|[\mathbf{f}]_k|^2\}$, and $\mathbf{w}\triangleq[w_1,\ldots w_K]$. Note that the expectations are taken with respect to the rays' directions $\theta_{l,m}$s and their complex amplitudes $\alpha_{l,m}$s. Mathematically speaking, we have to solve the following optimization problem:

$$\begin{aligned}\min_{\mathbf{w}}\ & \mathbf{w}^H\mathrm{E}\left\{\mathbf{H}_{\bar{1}}\mathbf{P}_{\bar{1}}\mathbf{H}_{\bar{1}}^H\right\}\mathbf{w}+\sigma_{n_t}^2\mathbf{w}^H\mathbf{\Sigma}\mathbf{w}+\sigma_{n_r}^2\\ \text{s.t}\quad & \mathbf{w}^H\mathrm{E}\left\{\mathbf{h}_1\mathbf{h}_1^H\right\}\mathbf{w}=1,\end{aligned}\tag{1}$$

It is straightforward to show that the optimum solution of (1) is a scaled version of the principal eigenvector of the matrix $\left(\mathrm{E}\left\{\mathbf{H}_{\bar{1}}\mathbf{P}_{\bar{1}}\mathbf{H}_{\bar{1}}^H\right\}+\sigma_{n_t}^2\mathbf{\Sigma}\right)^{-1}\mathrm{E}\left\{\mathbf{h}\mathbf{h}^H\right\}$ so as to satisfy the constraint in (1). To the best of our knowledge, this eigenvector cannot be obtained in a closed-form but could be numerically evaluated. However, besides being computationally demanding, this task must be performed by a central processor with global knowledge of all network parameters. The considered network lacks, unfortunately, such a processor.

III. Proposed CB solution

In this section, we prove under mild conditions that it is possible to derive an optimal solution of (1) in closed-form. To this end, we exploit useful approximations of the matrices $\mathrm{E}\left\{\mathbf{h}_1\mathbf{h}_1^H\right\}$ and $\mathrm{E}\left\{\mathbf{H}_{\bar{1}}\mathbf{P}_{\bar{1}}\mathbf{H}_{\bar{1}}^H\right\}$ that have the additional benefit of reducing by the same token the complexity of our CB optimization problem. As such, recurring to assumption A1, we have

$$\mathrm{E}\left\{\mathbf{h}_m\mathbf{h}_m^H\right\}=\int_{\Theta_m}p_m(\theta)\mathbf{a}(\phi_m+\theta)\mathbf{a}^H(\phi_m+\theta)d\theta,\tag{2}$$

where $\mathbf{a}(\theta)\triangleq[[\mathbf{a}(\theta)]_1\ldots[\mathbf{a}(\theta)]_K]^T$ with $[\mathbf{a}(\theta)]_k=[\mathbf{f}]_k e^{-j(2\pi/\lambda)r_k\cos(\theta-\psi_k)}$ and Θ_m is the span of the pdf $p_m(\theta)$ over which the integral is calculated. When the AS σ_m is relatively small, small angular deviations of $\theta_{l,m}$s occur and, hence, the Taylor series expansion of $\mathbf{a}(\phi_m+\theta)$ at ϕ_m yields

$$\mathbf{a}(\phi_m+\theta)\simeq\mathbf{a}(\phi_m)+\mathbf{a}'(\phi_m)\theta+\mathbf{a}''(\phi_m)\frac{\theta^2}{2},\tag{3}$$

where $\mathbf{a}'(\theta)$ and $\mathbf{a}''(\theta)$ are, respectively, the first and the second derivatives of $\mathbf{a}(\theta)$. After substituting (3) in (2) and integrating in the latter, we have

$$\mathrm{E}\left\{\mathbf{h}_m\mathbf{h}_m^H\right\}\simeq\frac{\mathbf{a}(\phi_m+\sigma_m)\mathbf{a}(\phi_m+\sigma_m)^H+\mathbf{a}(\phi_m-\sigma_m)\mathbf{a}(\phi_m-\sigma_m)^H}{2},\tag{4}$$

It is noteworthy that the result in (4) also holds with strict equality in the case of bichromatic (i.e., two-ray) channels (i.e., $L_m=2$) with rays located at angles σ_m and $-\sigma_m$ where the channel gain from the m-th source to the k-th terminal is

$$\left[\mathbf{g}_m^{(2)}\right]_k=\alpha_{1,m}e^{j\frac{2\pi}{\lambda}r_k\cos(\phi_m+\sigma_m-\psi_k)}+\alpha_{2,m}e^{j\frac{2\pi}{\lambda}r_k\cos(\phi_m-\sigma_m-\psi_k)}.\tag{5}$$

Consequently, when the AS is typically small to moderate, the polychromatic channel $\mathbf{g}_m$ could be substituted with the bichormatic channel $\mathbf{g}_m^{(2)}$. It holds from (4) that $\mathrm{E}\left\{\mathbf{h}_1\mathbf{h}_1^H\right\}=\frac{1}{2}\mathbf{\Xi}$ and $\mathrm{E}\left\{\mathbf{H}_{\bar{1}}\mathbf{P}_{\bar{1}}\mathbf{H}_{\bar{1}}^H\right\}\mathbf{\Gamma}\mathbf{\Lambda}\mathbf{\Gamma}^H$ where $\mathbf{\Xi}=\mathbf{a}(\sigma_1)\mathbf{a}(\sigma_1)^H+\mathbf{a}(-\sigma_1)\mathbf{a}(-\sigma_1)^H$, $\mathbf{\Gamma}=\left[\mathbf{a}(\tilde{\phi}_3),\mathbf{a}(\tilde{\phi}_4),\ldots,\mathbf{a}(\tilde{\phi}_{2M})\right]$ with $\tilde{\phi}_m=\phi_{m/2}-\sigma_{m/2}$ if m is even and $\tilde{\phi}_m=\phi_{(m-1)/2+1}+\sigma_{(m-1)/2+1}$ if m is odd, and $\mathbf{\Lambda}=(1/2)\,[p_2,p_2,\ldots,p_M,p_M]$. Therefore, when

In the Gaussian and Uniform distribution cases, $\Theta_m=[-\inf,+\inf]$ and $\Theta_m=[-\sqrt{3}\sigma_{\theta m},+\sqrt{3}\sigma_{\theta m}]$, respectively.

$\sigma_m,\ m=1,\dots,M$ are relatively small, (1) could be rewritten as

$$\max_{\boldsymbol{\gamma}} \frac{\boldsymbol{\gamma}^H \tilde{\boldsymbol{\Xi}} \boldsymbol{\gamma}}{\boldsymbol{\gamma}^H \boldsymbol{\gamma}} \quad \text{s.t.} \quad \boldsymbol{\gamma}^H \tilde{\boldsymbol{\Xi}} \boldsymbol{\gamma} = 2, \tag{6}$$

where $\boldsymbol{\gamma} = \boldsymbol{\Delta}^{\frac{1}{2}}\mathbf{w}$, $\boldsymbol{\Delta} = \boldsymbol{\Gamma}\boldsymbol{\Lambda}\boldsymbol{\Gamma}^H + \sigma_{n_t}^2\boldsymbol{\Sigma}$, and $\tilde{\boldsymbol{\Xi}} = \boldsymbol{\Delta}^{-\frac{1}{2}}\boldsymbol{\Xi}\boldsymbol{\Delta}^{-\frac{1}{2}}$. It is straightforward to show that the optimum solution of (6) is the principal eigenvector of the matrix $\tilde{\boldsymbol{\Xi}}$ scaled to satisfy the constraint in (6). Since $\boldsymbol{\Delta}^{-\frac{1}{2}}$ is a full-rank matrix, $\tilde{\boldsymbol{\Xi}}$ has the same rank as $\boldsymbol{\Xi}$ that is inferior or equal to two. Therefore, $\tilde{\boldsymbol{\Xi}}$ has at most two eigenvectors. In the sequel, we will prove that both $\boldsymbol{\Delta}^{-\frac{1}{2}}\left(\mathbf{a}(\sigma_1)+\mathbf{a}(-\sigma_1)\right)$ and $\boldsymbol{\Delta}^{-\frac{1}{2}}\left(\mathbf{a}(\sigma_1)+\mathbf{a}(-\sigma_1)\right)$ are eigenvectors of $\tilde{\boldsymbol{\Xi}}$. First, let us use the matrix inversion lemma to break $\boldsymbol{\Delta}^{-1}$ into several terms and, hence, obtain

$$\begin{aligned}
&\tilde{\boldsymbol{\Xi}}\boldsymbol{\Delta}^{-\frac{1}{2}}\left(\mathbf{a}(\sigma_1)\pm\mathbf{a}(-\sigma_1)\right) = \frac{K}{\sigma_{n_t}^2}\times \\
&\Big(\boldsymbol{\Delta}^{-\frac{1}{2}}\mathbf{a}(\sigma_1)\Big(1+\chi-\boldsymbol{\chi}(\sigma_1)^H\mathbf{D}^{-1}\Big(\boldsymbol{\chi}(\sigma_1)+\boldsymbol{\chi}(-\sigma_1)\Big)\Big)\pm \\
&\boldsymbol{\Delta}^{-\frac{1}{2}}\mathbf{a}(-\sigma_1)\Big(1+\chi^*-\boldsymbol{\chi}(-\sigma_1)^H\mathbf{D}^{-1}\Big(\boldsymbol{\chi}(\sigma_1)+\boldsymbol{\chi}(-\sigma_1)\Big)\Big)\Big),
\end{aligned} \tag{7}$$

where $\chi = \left(\mathbf{a}^H(\sigma_1)\boldsymbol{\Sigma}^{-1}\mathbf{a}(-\sigma_1)\right)/K$, $\boldsymbol{\chi}(\theta) = \left(\boldsymbol{\Gamma}^H\boldsymbol{\Sigma}^{-1}\mathbf{a}(\theta)\right)/K$, and $\mathbf{D} = \left(\sigma_{n_t}^2\boldsymbol{\Lambda}^{-1}+\boldsymbol{\Gamma}^H\boldsymbol{\Sigma}^{-1}\boldsymbol{\Gamma}\right)/K$. Now, we introduce the important theorem below.

Theorem 1: When the number of terminals K is relatively large, we have

$$\mathbf{a}(x)^H\boldsymbol{\Sigma}^{-1}\mathbf{a}(y) \xrightarrow{p1} 2\frac{J_1(\gamma(x-y))}{\gamma(x-y)}, \tag{8}$$

where $\gamma(\phi) \triangleq 4\pi(R/\lambda)\sin(\phi/2)$.

Proof: It follows from the definition of $\mathbf{a}(\theta)$ that $(\mathbf{a}(x)^H\boldsymbol{\Sigma}^{-1}\mathbf{a}(y))/K = (1/K)\sum_{k=1}^{K} e^{j\gamma(x-y)z_k}$ where $z_k,\ k=1,\dots,K$ are i.i.d compound random variables with the pdf $f_{z_k}(z) = \frac{2}{\pi}\sqrt{1-z^2}$ for $-1 \le z \le 1$. Using the strong law of large numbers and the fact that $(2/\pi)\int_{-1}^{1} e^{j\gamma(\phi)z}\sqrt{1-z^2}dz = 2J_1\left(\gamma\left(\phi\right)\right)/\gamma\left(\phi\right)$, we obtain (8).

It can be then inferred from this theorem that for large K, we have $\chi \xrightarrow{p1} 2\frac{J_1(\gamma(2\sigma_1))}{\gamma(2\sigma_1)}$, $\boldsymbol{\chi}(\theta) \xrightarrow{p1} 2\mathbf{z}(\theta)$, and $\mathbf{D} \xrightarrow{p1} 2\mathbf{Q}$ where $\mathbf{Q}$ is a $(2M-2)\times(2M-2)$ matrix with $[\mathbf{Q}]_{mn} = J_1(\gamma(\tilde{\phi}_{m+2}-\tilde{\phi}_{n+2}))/\gamma(\tilde{\phi}_{m+2}-\tilde{\phi}_{n+2})$ if $m \neq n$ and $[\mathbf{Q}]_{mn} = 1/2$ otherwise, and $\mathbf{z}(\theta)$ is a $(2M-2)\times 1$ vector with $[\mathbf{z}(\theta)]_m = J_1(\gamma(\theta-\tilde{\phi}_{m+2}))/\gamma(\theta-\tilde{\phi}_{m+2})$ if $\theta \neq \tilde{\phi}_{m+2}$ and $[\mathbf{z}(\theta)]_m = 1/2$ otherwise. When $\sigma_m,\ m=1,\dots,M$ are relatively small, we have $\mathbf{z}(\sigma_1) \simeq \mathbf{z}(-\sigma_1)$ and, hence, it holds that, for large K, the eigenvalues associated with $\boldsymbol{\Delta}^{-\frac{1}{2}}\left(\mathbf{a}(\sigma_1)+\mathbf{a}(-\sigma_1)\right)$ and $\boldsymbol{\Delta}^{-\frac{1}{2}}\left(\mathbf{a}(\sigma_1)-\mathbf{a}(-\sigma_1)\right)$ are $\rho_1(\sigma_1) \simeq \frac{K}{\sigma_{n_t}^2}\left(1+2\frac{J_1(\gamma(2\sigma_1))}{\gamma(2\sigma_1)}-4\mathbf{z}(\sigma_1)^T\mathbf{Q}^{-1}\mathbf{z}(\sigma_1)\right)$ and $\rho_2(\sigma_1) \simeq \frac{K}{\sigma_{n_t}^2}\left(1-2\frac{J_1(\gamma(2\sigma_1))}{\gamma(2\sigma_1)}\right)$, respectively. What remains to be done to find the principal eigenvector of $\tilde{\boldsymbol{\Xi}}$ is then comparing the eigenvalues ρ_1 and ρ_2. As such, we introduce the theorem below.

Theorem 2: When the number of terminals K is relatively large, we have

$$2\mathbf{z}(0)^T\mathbf{Q}^{-1}\mathbf{z}(0) \in [0,1[. \tag{9}$$

Proof: It follows from A2 and the above results that

$$2\mathbf{z}(0)^T\mathbf{Q}^{-1}\mathbf{z}(0) = \lim_{K\to\infty}\frac{1}{K}\|\mathbf{P}\mathbf{a}(0)\|^2, \tag{10}$$

where $\mathbf{P} = \boldsymbol{\Gamma}(\boldsymbol{\Gamma}^H\boldsymbol{\Gamma})^{-1}\boldsymbol{\Gamma}^H$ is the orthogonal projection matrix onto the subspace spanned by the columns of $\boldsymbol{\Gamma}$. $\mathbf{P}\mathbf{a}(0)$ is then the projection of $\mathbf{a}(0)$ into the latter subspace and, hence, $0 \le 2\mathbf{z}(0)^T\mathbf{Q}^{-1}\mathbf{z}(0) \le \|\mathbf{a}(0)\| = 1$. While the left-hand side (LHS) inequality holds with equality if $\mathbf{a}(0)$ is orthogonal to the column span of $\boldsymbol{\Gamma}$, the right-hand side (RHS) inequality holds with equality if $\mathbf{a}(0)$ is in the column span of $\boldsymbol{\Gamma}$. The latter event is, however, highly unlikely when K is large and, hence, $2\mathbf{z}(0)^T\mathbf{Q}^{-1}\mathbf{z}(0)$ is strictly inferior to 1.

Using Theorem 2, one can readily show that $\lim_{\sigma_1\to 0}\left(\rho_1-\rho_2\right)\left(\sigma_1\right) > 0$. Therefore, there exists a real κ such that if σ_1 is small enough we have $\sigma_1 < \kappa$ then $\rho_1(\sigma_1) > \rho_2(\sigma_1)$. Consequently, for relatively small $\sigma_m,\ m=1,\dots,M$ and large K, $\boldsymbol{\Delta}^{-\frac{1}{2}}\left(\mathbf{a}(\sigma_1)+\mathbf{a}(-\sigma_1)\right)$ is the principal eigenvector of $\tilde{\boldsymbol{\Xi}}$. Finally, scaling $\boldsymbol{\Delta}^{-1}(\mathbf{a}(\sigma_1)+\mathbf{a}(-\sigma_1))$ to satisfy the constraint in (6) and breaking $\boldsymbol{\Delta}^{-1}$ into several terms, we show for relatively small $\sigma_m,\ m=1,\dots,M$ and large K that the optimal solution of (1) is given by

$$\mathbf{w}_{\mathrm{BD}} = \frac{\boldsymbol{\Sigma}^{-1}\left(\mathbf{a}\left(\sigma_1\right)+\mathbf{a}\left(-\sigma_1\right)-\boldsymbol{\Gamma}\mathbf{Q}^{-1}\boldsymbol{\nu}(\sigma_1)\right)}{K\left(1+2\frac{J_1(\gamma(2\sigma_1))}{\gamma(2\sigma_1)}-\boldsymbol{\nu}(\sigma_1)^T\mathbf{Q}^{-1}\boldsymbol{\nu}(\sigma_1)\right)}, \tag{11}$$

where $\boldsymbol{\nu}(\sigma_1) = \mathbf{z}(\sigma_1)+\mathbf{z}(-\sigma_1)$. Note that we denote this CB solution by $\mathbf{w}_{\mathrm{BD}}$ since it relies on the *bichromatic* approximation in (4) and, further, lends itself to a *distributed* implementation, as we will shortly see below. It can be observed from (11) that the k-th terminal's weight $[\mathbf{w}_{\mathrm{BD}}]_k$ depends, according to A4, on the information locally available at this node as well as $\sigma_m,\ m=1,\dots,M$ and $\phi_m,\ m=1,\dots,M$, which could be estimated at the sources and broadcasted to the network. Therefore, each terminal is able to autonomously compute its weight without requiring any information exchange with the other terminals in the network. This is in fact a very desired feature for any CB solution since it enables its distributed implementation and, hence, avoids any additional overhead due to such an exchange. Furthermore, from (11), $\mathbf{w}_{\mathrm{BD}}$ is independent of $p_m(\theta), m=1,\dots,M$. This is also an outstanding feature which allows the proposed bichromatic distributed CB (B-DCB)'s implementation in any scattered environment regardless of its scattering distribution.

In the sequel, we compare in performance the proposed B-DCB with the two main conventional types of CB solutions disclosed so far in the literature, namely MCB and OCB [5].

IV. Performance analysis under ideal conditions

A. CB performance metrics

Let $\xi_{\mathbf{w}}$ denote the achieved signal-to-interference-plus-noise ratio (SINR) using $\mathbf{w}$ and given by $\xi_{\mathbf{w}} = \left|\mathbf{w}^H\mathbf{h}_1 s_1\right|^2 / \left|\mathbf{w}^H\mathbf{H}_{\bar{1}}\mathbf{s}_{\bar{1}}+\mathbf{w}^H(\mathbf{f}\odot\mathbf{n}_t)+n_r\right|^2$. $\xi_{\mathbf{w}}$ is then an excessively complex function of the random variables n_r, $[\mathbf{n}_t]_k$, r_k, ψ_k and $[\mathbf{f}]_k$ for $k=1,\dots,K$ and $\alpha_{l,m}$ and $\theta_{l,m}$ $l=1,\dots,L_m$ for $m=1,\dots M$ and, hence, a random quantity of its own. Therefore, it is more practical to compare the CB solutions in

terms of achieved average-signal-to-average-interference-plus-noise ratio (ASAINR) defined for any $\mathbf{w}$ as $\tilde{\xi}_{\mathbf{w}} = p_1 \mathrm{E}\left\{\left|\mathbf{w}^H\mathbf{h}_1\right|^2\right\} / \mathrm{E}\left\{\mathbf{w}^H\mathbf{H}_{\bar{1}}\mathbf{P}_{\bar{1}}\mathbf{H}_{\bar{1}}^H\mathbf{w} + \sigma_{n_t}^2\mathbf{w}^H\mathbf{\Sigma}\mathbf{w}\right\} + \sigma_{n_r}^2$. Despite being a more adequate performance metric, please note that the ASINR $\bar{\xi}_{\mathbf{w}} = \mathrm{E}\{\xi_{\mathbf{w}}\}$ cannot be adopted hereafter since, to the best of our knowledge, it appears to be untractable in closed-form.

B. ASAINR gain of B-DCB vs. MCB

It can be shown that the ASAINR achieved by B-DCB is given by as shown on the top of the next page where

$$\Psi(\phi_m) = \int_{\Theta_m} p_m(\theta) \left(\frac{J_1(\gamma(\phi_m+\theta+\sigma_1))}{\gamma(\phi_m+\theta+\sigma_1)} + \frac{J_1(\gamma(\phi_m+\theta-\sigma_1))}{\gamma(\phi_m+\theta-\sigma_1)} - \mathbf{z}(\phi_m+\theta)^T \mathbf{Q}^{-1}\boldsymbol{\nu}(\sigma_1) \right)^2 d\theta,\ m = 1, \ldots, M. \quad (13)$$

Moreover, when there is no scattering (i.e., $\sigma_m = 0,\ m = 1, \ldots, M$), we have $\mathbf{z}(\phi_n) = \mathbf{Q}\mathbf{e}_{2n-2}$ and, therefore,

$$\mathbf{z}(\phi_n)^T\mathbf{Q}^{-1}\boldsymbol{\nu}(\sigma_1) = \frac{J_1(\gamma(\phi_n+\sigma_1))}{\gamma(\phi_n+\sigma_1)} + \frac{J_1(\gamma(\phi_n-\sigma_1))}{\gamma(\phi_n-\sigma_1)}. \quad (14)$$

Substituting (14) in (13), we obtain in such a case $\Psi(\phi_m) = 0$ for $m = 1, \ldots, M$ and, hence, (12) boils down to

$$\tilde{\xi}_{\mathbf{w}_{\mathrm{BD}}} = \frac{p_1\left(1 + 2\mathbf{z}(0)^T\mathbf{Q}^{-1}\mathbf{z}(0)\left(\frac{1}{K} - 1\right)\right)}{\sum_{m=2}^{M}\frac{p_m}{K} + \frac{\sigma_{n_t}^2}{K} + \sigma_{n_r}^2\left(1 - 2\mathbf{z}(0)^T\mathbf{Q}^{-1}\mathbf{z}(0)\right)}. \quad (15)$$

As can be observed from (15), $\tilde{\xi}_{\mathbf{w}_{\mathrm{BD}}}$ is an increasing function of K that asymptotically approaches $\tilde{\xi}^{\max} = p1/\sigma_{n_r}^2$. Note that $\tilde{\xi}^{\max}$ is the maximum ASAINR ever achievable only when the desired power is kept constant to p_1 and the undesired one is reduced to its minimum level ever, i.e., $\sigma_{n_r}^2$, that is only by entirely nulling all the interferers. Simulations in Section V will show that $\tilde{\xi}_{\mathbf{w}_{\mathrm{BD}}} \simeq \tilde{\xi}^{\max}$ when $\sigma_m\ m = 1, \ldots, M$ are relatively small to moderate in lightly- to moderately-scattered environments, respectively. This further proves the efficiency of the proposed B-DCB.

Now, let us turn our attention to the ASAINR achieved by MCB $\tilde{\xi}_{\mathbf{w}_{\mathrm{M}}}$. To the best of our knowledge, $\tilde{\xi}_{\mathbf{w}_{\mathrm{M}}}$ is intractable in closed-form hampering thereby its rigorous analytical study. Nevertheless, it can be shown for large K that

$$\tilde{\xi}_{\mathbf{w}_{\mathrm{M}}} \simeq \frac{p_1\Psi_{\mathrm{M}}(0)}{\sum_{m=2}^{M} p_m\Psi_{\mathrm{M}}(\phi_m) + \frac{\sigma_{n_r}^2}{4}\left(1 - 2\boldsymbol{\nu}_{\mathrm{M}}^T(0)\mathbf{Q}_{\mathrm{M}}^{-1}\boldsymbol{\nu}_{\mathrm{M}}(0)\right)^2}, \quad (16)$$

where

$$\Psi_{\mathrm{M}}(\phi_m) = \int_{\Theta_m} p_m(\theta)\left(\frac{J_1(\gamma(\phi_m+\theta))}{\gamma(\phi_m+\theta)} - \boldsymbol{\nu}_{\mathrm{M}}^T(\phi_m+\theta)\mathbf{Q}_{\mathrm{M}}^{-1}\boldsymbol{\nu}_{\mathrm{M}}(0)\right)^2 d\theta, \quad (17)$$

$\mathbf{Q}_{\mathrm{M}}$ is a $(M-1)\times(M-1)$ matrix with $[\mathbf{Q}_{\mathrm{M}}]_{mn} = J_1(\gamma(\phi_{m+1} - \phi_{n+1}))/\gamma(\phi_{m+1} - \phi_{n+1})$, and $\boldsymbol{\nu}_{\mathrm{M}}(\theta)$ is a $(M-1)\times 1$ vector with $[\boldsymbol{\nu}_{\mathrm{M}}(\theta)]_m = J_1(\gamma(\theta - \phi_{m+1}))/\gamma(\theta - \phi_{m+1})$.

It follows from (12) and (16) that if there is no scattering (i.e., $\sigma_m = 0,\ m = 1, \ldots, M$), we have $\Upsilon(\mathbf{w}_{\mathrm{M}}) \simeq 1$, when K is large enough. This means that, in such a case, MCB is also able to achieve the maximum achievable ASAINR $\tilde{\xi}^{\max}$. This is expected since the monochromatic assumption made to derive $\mathbf{w}_{\mathrm{M}}$ becomes valid when $\sigma_m = 0,\ m = 1, \ldots, M$. Note that even though B-DCB and MCB achieve the same ASAINR in the absence of scattering, the former still keeps a precious practical implementation advantage over the latter by its distributed nature.

$$\gamma\left(\tilde{\phi}_m - \tilde{\phi}_n\right) \gg \frac{3}{4} \quad m, n = 1, \ldots, 2M,\ \ m \neq n, \quad (18)$$

then we have

$$\frac{J_1\left(\gamma\left(\tilde{\phi}_m - \tilde{\phi}_n\right)\right)}{\gamma\left(\tilde{\phi}_m - \tilde{\phi}_n\right)} = \sqrt{\frac{2}{\pi}}\frac{\cos\left(\gamma\left(\tilde{\phi}_m - \tilde{\phi}_n\right) - \frac{3\pi}{4}\right)}{\gamma\left(\tilde{\phi}_m - \tilde{\phi}_n\right)}, \quad (19)$$

and, hence, $[\boldsymbol{\nu}(\sigma_1)]_m \simeq 0,\ m = 1, \ldots, 2M$ and $[\boldsymbol{\nu}_{\mathrm{M}}(0)]_m \simeq 1,\ m = 1, \ldots, M$. Therefore, it holds that $\boldsymbol{\nu}(\sigma_1)^T\mathbf{Q}^{-1}\boldsymbol{\nu}(\sigma_1) \ll 1$ and $\boldsymbol{\nu}_{\mathrm{M}}^T(0)\mathbf{Q}_{\mathrm{M}}^{-1}\boldsymbol{\nu}_{\mathrm{M}}(0) \ll 1$. Besides, if $\sigma_m,\ m = 2, \ldots, M$ are relatively small, i.e., in lightly- to moderately-scattered environments, one could easily show that both $\Psi(\phi_m) \simeq 0$ and $\Psi_{\mathrm{M}}(\phi_m) \simeq 0,\ m = 1, \ldots, M$. Consequently, the ASAINR gain of MCB against B-DCB boils down to $\Upsilon(\mathbf{w}_{\mathrm{M}}) \simeq \Psi_{\mathrm{M}}(0)\left(1 + 2J_1(\gamma(2\sigma_1))/\gamma(2\sigma_1)\right)^2/\Psi(0)$ for any σ_1 and large K. In particular, when σ_1 is also small, the Taylor series expansion of $J_1(\gamma(\theta \pm \sigma_1))/\gamma(\theta \pm \sigma_1)$ at θ yields

$$\frac{J_1(\gamma(\theta \pm \sigma_1))}{\gamma(\theta \pm \sigma_1)} = \frac{J_1(\gamma(\theta))}{\gamma(\theta)} \pm \sigma_1\left(\frac{J_1(\gamma(x))}{\gamma(x)}\right)'\Big|_{x=\theta}, \quad (20)$$

and, hence, $\Psi(0) \simeq 4\Psi_{\mathrm{M}}(0)$. Accordingly, it holds for large K that

$$\Upsilon(\mathbf{w}_{\mathrm{M}}) \simeq \frac{1}{4}\left(1 + {}_0F_1\left(;2;-4\pi^2\left(\frac{R}{\lambda}\right)^2\sigma_1^2\right)\right)^2, \quad (21)$$

where ${}_0F_1\left(;2;-4\pi^2\left(\frac{R}{\lambda}\right)^2 x^2\right)$ is the hypergeometric function strictly decreasing at x near 0. When σ_ms are relatively small in lightly- to moderately-scattered environments, the ASAINR gain of $\mathbf{w}_{\mathrm{BD}}$ against $\mathbf{w}_{\mathrm{M}}$ derived without accounting for scattering increases with σ_1. This proves the importance of accounting for scattering when designing the proposed B-DCB.

C. ASAINR gain of B-DCB vs. OCB

It can be shown for large L_1 that $\tilde{\xi}_{\mathbf{w}_{\mathrm{O}}} = \frac{p_1}{\frac{\sigma_{n_t}^2}{K} + \sigma_{n_r}^2}$. This result implies that $\tilde{\xi}_{\mathbf{w}_{\mathrm{O}}} \simeq \tilde{\xi}^{\max}$ for large K regardless of $p_m(\theta)$ and $\sigma_m,\ m = 1, \ldots, M$. Therefore, OCB is able to achieve as expected the maximum achievable ASAINR in lightly-, moderately-, and even highly-scattered environments. As discussed above, since the proposed B-DCB also achieves $\tilde{\xi}^{\max}$ when $\sigma_m,\ m = 1, \ldots, M$ are small in lightly- to moderately-scattered environments, then $\Upsilon(\mathbf{w}_{\mathrm{O}}) \simeq 1$ holds when K is large enough. However, for large σ_1 in highly-scattered environments, if (18) is satisfied, we have for large K $\Upsilon(\mathbf{w}_{\mathrm{O}}) \simeq \frac{1}{\Psi(0)} \geq 1$. The inequality is due to the fact that $J_1(x)/(x) \leq 1/2$ for any real x. As can be observed from teh above result, OCB outperforms B-DCB when σ_1 is large in highly-scattered environments. Furthermore, the ASAINR gain of OCB against B-DCB increases with σ_1, since $\Psi(0)$ is a decreasing function of the latter. Actually, we will later show numerically in Section V that these observations hold as well when $\sigma_m,\ m = 1, \ldots, M$ are large in highly-scattered environments. Although OCB stands out to be the most efficient CB solution under ideal conditions, we will prove in the next section that it severely deteriorates in performance under

$$\tilde{\xi}_{\mathbf{w}_{\mathrm{BD}}}=\frac{p_1\Big(1+(2(K-1)\,\Psi\,(0))/\Big(1+2\frac{J_1(\gamma(2\sigma_1))}{\gamma(2\sigma_1)}-\boldsymbol{\nu}(\sigma_1)^T\mathbf{Q}^{-1}\boldsymbol{\nu}(\sigma_1)\Big)\Big)}{\sum_{m=2}^{M}p_m\Big(1+(2(K-1)\Psi\,(\phi_m))/\Big(1+2\frac{J_1(\gamma(2\sigma_1))}{\gamma(2\sigma_1)}-\boldsymbol{\nu}(\sigma_1)^T\mathbf{Q}^{-1}\boldsymbol{\nu}(\sigma_1)\Big)\Big)+\sigma_{n_t}^2+\frac{\sigma_{n_r}^2K}{2}\Big(1+2\frac{J_1(\gamma(2\sigma_1))}{\gamma(2\sigma_1)}-\boldsymbol{\nu}(\sigma_1)^T\mathbf{Q}^{-1}\boldsymbol{\nu}(\sigma_1)\Big)}. \quad (12)$$

real-world conditions to become less efficient than the proposed B-DCB even in highly-scattered environments.

V. Simulation Results

Computer simulations are provided to support the theoretical results. All empirical average quantities are calculated over 10^6 random realizations of r_k, ψ_k, $[\mathbf{f}]_k$ for $k=1,\ldots,K$ and $\alpha_{l,m}$, $\theta_{l,m}$ for $l=1,\ldots,L_m$. In all simulations, all sources have the same power $p=1$ and $\sigma_{n_r}^2=\sigma_{n_t}^2=1$. The number of rays is $L_m=6$, $\sigma_m=\sigma$ and the scattering distribution $p_m(\theta)$ is Uniform for $m=1,\ldots,M$, except in Fig. 2(b) where we consider a Gaussian distribution. Unless otherwise stated, $K=20$ and $M_I=3$ with $[\phi_2,\phi_3,\phi_4]=[10,15,20]$ degrees.

Fig. 2 plots, under ideal conditions, the ASAINRs $\tilde{\xi}_{\mathbf{w}_{\mathrm{BD}}}$, $\tilde{\xi}_{\mathbf{w}_{\mathrm{M}}}$, and $\tilde{\xi}_{\mathbf{w}_{\mathrm{O}}}$ and the ASINRs $\bar{\xi}_{\mathbf{w}_{\mathrm{BD}}}$, $\bar{\xi}_{\mathbf{w}_{\mathrm{M}}}$, and $\bar{\xi}_{\mathbf{w}_{\mathrm{O}}}$ versus σ. The scattering distributions $p_m(\theta), m=1,\ldots,M$ are assumed to be Uniform in Fig. 2(a) and Gaussian in Fig. 2(b). From these figures, we confirm that the analytical $\tilde{\xi}_{\mathbf{w}_{\mathrm{BD}}}$ and $\tilde{\xi}_{\mathbf{w}_{\mathrm{O}}}$ match perfectly their empirical counterparts while (16) closely approaches the empirical $\tilde{\xi}_{\mathbf{w}_{\mathrm{BD}}}$ for $K=20$. Both figures show that, under ideal conditions, OCB is able to reach the maximum achievable ASAINR $\tilde{\xi}^{\max}$, regardless of σ. This is due to the optimality of such a CB solution. Figs. 2(a) and 2(b) also show that the ASAINR $\tilde{\xi}_{\mathbf{w}_{\mathrm{BD}}}$ achieved by the proposed B-DCB approaches $\tilde{\xi}_{\max}$ in lightly to moderately-scattered environments where σ is in the range of 17 degrees. When the scattering distributions are Uniform, this means that the angle deviations $\theta_{l,m}$s vary from approximately -30 to 30 degrees (i.e., an angular interval of almost 60 degrees). Consequently, in lightly to moderately-scattered environments, the proposed B-DCB is also optimal. However, the ASAINR $\tilde{\xi}_{\mathbf{w}_{\mathrm{BD}}}$ achieved by B-DCB severely deteriorates in highly-scattered environments where $\sigma>20$ degrees. Furthermore, we see from Figs. 2(a) and 2(b) that the ASAINR performed by MCB, which is designed without accounting for scattering, slightly decreases in lightly-scattered environments where σ is around 5 degrees, and becomes soon unsatisfactory in moderately- to highly-scattered environments. In such settings, the proposed B-DCB is able to achieve until 6 dB of ASAINR gain against MCB. All these observations corroborate the analytical results of Section IV-B. Moreover, from these figures, the curves of $\tilde{\xi}_{\mathbf{w}_{\mathrm{O}}}$, $\tilde{\xi}_{\mathbf{w}_{\mathrm{BD}}}$, and $\tilde{\xi}_{\mathbf{w}_{\mathrm{M}}}$ are almost indistinguishable from $\bar{\xi}_{\mathbf{w}_{\mathrm{O}}}$, $\bar{\xi}_{\mathbf{w}_{\mathrm{BD}}}$, and $\bar{\xi}_{\mathbf{w}_{\mathrm{M}}}$, respectively, when $K=20$. This proves that the ASAINR is a meaningful performance measure.

VI. Conclusions

In this paper, a CB technique aiming to achieve a dual-hop communication from a source surrounded by M_I interferences to a receiver was considered. Its weights were designed so as to minimize the interferences plus noises' powers while maintaining the received power from the source to a constant level. We showed, however, that they are intractable in closed-form due to the complexity of the polychromatic channels arising from the presence of scattering. By recurring to a two-ray channel approximation proved valid at relatively low AS values, we were able to derive the new optimum weights and prove that they could be locally computed at each terminal, thereby complying with the distributed feature of the network of interest. The so-obtained B-DCB was then analyzed and compared in performance to both MCB and OCB. We showed that the proposed B-DCB always outperforms MCB and, further, its performance approaches that of OCB.

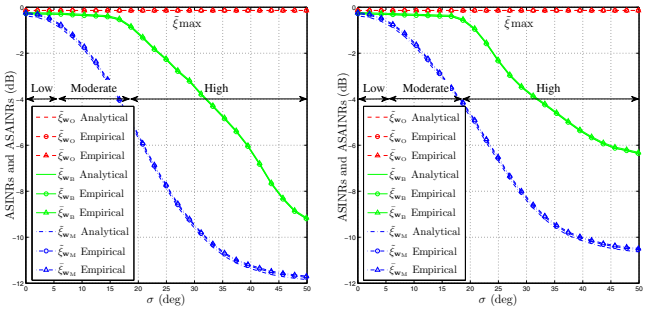

(a) Uniform distributions. (b) Gaussian distributions.

Fig. 2. The analytical and the empirical ASAINRs achieved, under ideal conditions, by MCB, OCB, and the proposed B-DCB as well as their empirical ASINRs versus σ for $K=20$ when the scattering distributions are (a): Uniform and (b): Gaussian.

References

[1] Y. Jing and H. Jafarkhani, " Network beamforming using relays with perfect channel information," *IEEE Trans. Inf. Theory,* vol. 55, pp. 2499-2517, June 2009.

[2] H. Shen, W. Xu, S. Jin, and C. Zhao, "Joint transmit and receive beamforming for MIMO downlinks with channel uncertainty," *IEEE Trans. Veh. Tech.,* vol. 63, pp. 2319-2335, June 2014.

[3] H.-B. Kong, C. Song, H. Park, and I. Lee, "A new beamforming design for MIMO AF relaying systems with direct link," *IEEE Trans. Commun.,* vol. 62, pp. 2286-2295, July 2014.

[4] S. Zaidi and S. Affes, "SNR and throughput analysis of distributed collaborative beamforming in locally-scattered environments," *Wiley J. Wireless Commun. and Mobile Comput.,* vol. 12, pp. 1620-1633, Dec. 2012. Invited Paper.

[5] S. Zaidi and S. Affes, "Analysis of collaborative beamforming designs in real-world environments," *Proc. IEEE WCNC'2013,* Shanghai, China, Apr. 7-10, 2013.

[6] D. J. Love, R. W. Heath, and T. Strohmer, "Grassmannian beamforming for multiple-input multiple-output wireless systems," *IEEE Trans. Inf. Theory,* vol. 49, pp. 2735-2747, Oct. 2003.

[7] H. Ochiai, P. Mitran, H. V. Poor, and V. Tarokh, "Collaborative beamforming for distributed wireless ad hoc sensor networks," *IEEE Trans. Signal Process.,* vol. 53, pp. 4110-4124, Nov. 2005.

[8] M. F. A. Ahmed and S. A. Vorobyov, "Collaborative beamforming for wireless sensor networks with Gaussian distributed sensor nodes," *IEEE Trans. Wireless Commun.,* vol. 8, pp. 638-643, Feb. 2009.

[9] L. Dong, A. P. Petropulu, and H. V. Poor, "A cross-layer approach to collaborative beamforming for wireless ad hoc networks," *IEEE Trans. Signal Process.,* vol. 56, pp. 2981-2993, July 2008.

[10] A. Amar, "The effect of local scattering on the gain and beamwidth of a collaborative beampattern for wireless sensor networks," *IEEE Trans. Wireless Commun.,* vol. 9, pp. 2730-2736, Sep. 2010.

[11] S. Zaidi and S. Affes "Distributed collaborative beamforming in the presence of angular scattering," *IEEE Trans. Commun.,* vol. 62, pp. 1668-1680, May 2014.

[12] S. Zaidi and S. Affes, "Distributed collaborative beamforming with minimum overhead for local scattering environments," *Proc. IEEE IWCMC'2012,* Cyprus, Aug. 27-31, 2012. Invited Paper.